

Alignment of Druglike Compounds in Lipid Bilayers Analyzed by Solid-State ^{19}F -NMR and Molecular Dynamics, Based on Dipolar Couplings of Adjacent CF_3 Groups

Ulrich H. N. Dürr,^{†,‡} Sergii Afonin,[†] Barbara Hoff,^{‡,§} Giuseppina de Luca,[§] James W. Emsley,[¶] and Anne S. Ulrich^{*,†}

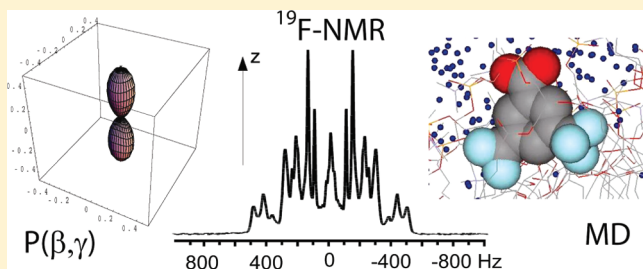
[†]Institute of Organic Chemistry and CFN, Institute of Biological Interfaces (IBG-2), Karlsruhe Institute of Technology (KIT), Fritz-Haber-Weg 6, 76131 Karlsruhe, Germany

[‡]Bioprocess Engineering, IMVM, Fritz-Haber-Weg 2, 76131 Karlsruhe, Germany

[§]Dipartimento di Chimica, University of Calabria, Campus di Arcavacata, Via Pietro Bucci Cubo 12C, I-87036 Rende (Cosenza), Italy

[¶]School of Chemistry, University of Southampton, Southampton SO17 1BJ, U.K.

ABSTRACT: Solid-state ^{19}F -NMR spectroscopy is frequently used to analyze the structure and dynamics of lipophilic drugs and peptides embedded in biomembranes. The homonuclear dipolar couplings of trifluoromethyl (CF_3) labels can provide valuable parameters such as orientational constraints and/or distances. To characterize the complex dipolar patterns of multiple ^{19}F spin interactions, three different model compounds carrying two CF_3 groups in *meta*-position on a phenyl ring were incorporated in macroscopically aligned DMPC bilayers. The dipolar patterns obtained with the CPMG (Carr–Purcell–Meiboom–Gill) multipulse sequence were analyzed to yield simultaneously the intra- CF_3 and intergroup dipolar coupling values. The fluorine–fluorine distances were predicted by a density functional calculation, and the alignment of the labeled molecular segment could be determined from these distances and the dipolar coupling values. The different compounds were found to align in the lipid bilayer according to their amphiphilic properties, though with a weak anisotropic preference that is typical of solutes in liquid crystals. The residual dipolar couplings were used to calculate Saupe order parameters. For the least complex molecule, $(\text{CF}_3)_2\text{-BA}$, an orientational probability function for the solute in the lipid matrix could be derived. The overall description of how $(\text{CF}_3)_2\text{-BA}$ is embedded in the bilayer was independently assessed by molecular dynamics simulations, and compared in structural and dynamical terms with the results of the NMR experiments.



1. INTRODUCTION

Solid-state NMR spectroscopy is a powerful approach for studying the interaction of labeled biomolecules with cell membranes. Especially fluorine, when used as a selective NMR label, is a highly sensitive nucleus that engages in strong dipolar interactions and does not suffer from any natural abundance background.^{1–10} Trifluoromethyl (CF_3) groups are particularly useful labels for measuring orientational constraints, as the homonuclear dipolar interactions within this group yield distinct triplet line shapes, with distinguishable positive and negative splittings and no need for chemical shift referencing in macroscopically oriented membrane samples.^{11,12} Many lipophilic drugs contain CF_3 groups, and the synthetic challenge of introducing selective CF_3 labels into polypeptides has also largely been solved.^{13–15} The accuracy of such solid-state ^{19}F -NMR approach to structure analysis was demonstrated to be comparable to that of using nonperturbing but far less sensitive ^2H -labels.^{16,17} In previous applications, numerous CF_3 -labeled peptides have thus been comprehensively characterized in terms of their conformational, orientational, and dynamic behavior in the lipid bilayer.^{16,18–24} For all these systems, a series of labeled

peptide analogues had to be measured one by one, each one carrying a single CF_3 group in different positions along the amino acid sequence. In order to proceed toward the simultaneous analysis of multiple CF_3 labels, there is now a need for new types of experiments and data analysis schemes. As a method for determining both local distances and orientations, it has already been demonstrated that the Carr–Purcell–Meiboom–Gill (CPMG) multipulse sequence can yield homonuclear dipolar couplings in static samples. These earlier studies were performed with molecules carrying two separate ^{19}F nuclei,²⁵ a single CF_3 group,²⁶ and two equivalent CF_3 groups.²⁷

The present work extends these studies toward a more complex spin system consisting of six ^{19}F nuclei, referred to as a “six-spin system”, in model compounds carrying two trifluoromethyl groups on an aromatic ring. We consider this situation of two CF_3 groups, interacting over an intermediate distance by dipolar coupling, as a good model for CF_3 -containing drugs and

Received: December 21, 2011

Revised: March 22, 2012

Published: March 22, 2012

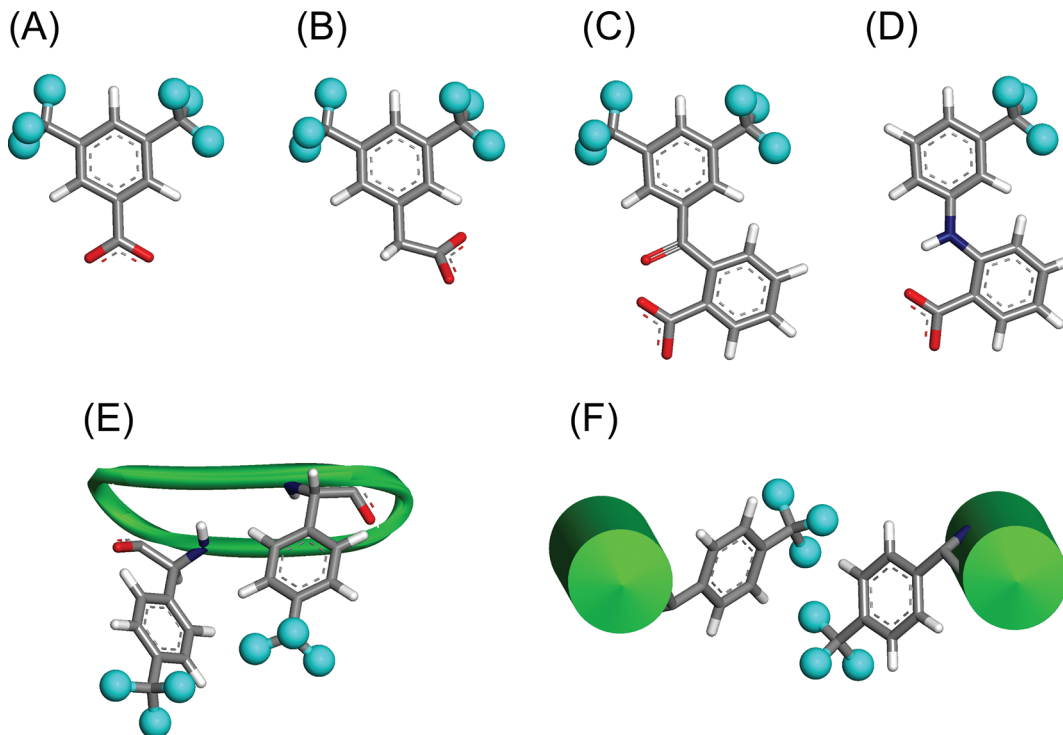


Figure 1. Molecular structures of the three six-spin systems examined in this study, and examples of molecular geometries that are similar to the investigated molecules. The compounds (A) $(\text{CF}_3)_2\text{-BA}$, (B) $(\text{CF}_3)_2\text{-PhA}$, and (C) $(\text{CF}_3)_2\text{-BBA}$, each carrying two CF_3 groups in *meta*-position, are investigated in the present study. (D) The drug flufenamic acid has a structure that is very similar to that of $(\text{CF}_3)_2\text{-BBA}$. (E) Gramicidin S, a cyclic decapeptide with antimicrobial activity, has been labeled with two CF_3 groups in order to study their dipolar interaction. (F) Likewise, two CF_3 groups can be used to report on the structure and dynamics of oligomeric assemblies, as illustrated for a hypothetical dimer of α -helices.

CF_3 -labeled biomolecules to be addressed in the future. Besides yielding orientational information, CF_3 groups are promising reporters of spatial proximity and may thus complement the CODEX spin-counting analysis based on spin diffusion between several single labels.²⁸ The high gyromagnetic ratio of the fluorine nucleus means that dipolar coupling between two CF_3 groups should be detectable for distances up to 12 Å or more.^{29,30} The feasibility of this approach has already been demonstrated in a study on the antimicrobial peptide gramicidin S which carried two equivalent CF_3 groups (ref 27 and Figure 1E). Analogously, single CF_3 groups on adjacent monomers within an oligomer may give direct evidence of molecular self-assembly, even from very basic NMR experiments (Figure 1F illustrates this hypothetical situation). For example, in the homotetrameric M2-TMP channel from influenza A virus, it was possible to detect ^{19}F -dipolar couplings between monomers that had been selectively labeled with ^{19}F -labeled tryptophan analogues.^{31,32} Changes in dipolar couplings were observed upon changing the pH value of the sample and could be correlated with the channel's gating behavior. By establishing here the selected six-spin compounds as model systems, we expect to gain valuable experience with complex dipolar coupling patterns between two CF_3 groups at intermediate distance.

The six-spin systems investigated here are presented in Figure 1A–C, along with three related molecular situations that illustrate their relevance, Figure 1D–F. All three molecules contain a pair of CF_3 groups in the *meta*-position on an aromatic ring. They also possess a carboxyl group, giving them a polar region that may assist in localizing and orienting them in the

amphiphilic region of a lipid membrane. The three model compounds differ in size and symmetry, which should influence their motional and alignment properties within the membrane. They will be referred to as $(\text{CF}_3)_2\text{-BA}$ (benzoic acid), $(\text{CF}_3)_2\text{-PhA}$ (phenylacetic acid), and $(\text{CF}_3)_2\text{-BBA}$ (benzoylbenzoic acid). The largest and least symmetric molecule, $(\text{CF}_3)_2\text{-BBA}$ (Figure 1C), is similar to the nonsteroidal anti-inflammatory drug flufenamic acid (Figure 1D), which carries a single CF_3 group and was the focus of previous studies.^{26,33} By acquiring and analyzing the ^{19}F -NMR spectra of $(\text{CF}_3)_2\text{-BBA}$, we intended to demonstrate the general potential for monitoring the behavior of related druglike compounds carrying two CF_3 groups. The two smaller and more symmetric molecules, $(\text{CF}_3)_2\text{-BA}$ (Figure 1A) and $(\text{CF}_3)_2\text{-PhA}$ (Figure 1B), were chosen for their less complex geometry, as they are ideally suited to investigate primarily the possible challenges involved in obtaining and analyzing their dipolar patterns. The simplest molecule, $(\text{CF}_3)_2\text{-BA}$, has also sufficient symmetry that the residual dipolar couplings obtained can even be used to calculate the principal Saupe order parameters, which in turn could be used to derive a probability distribution function describing how this molecule is oriented in the lipid bilayer. This experimental NMR information can then be compared with an independent molecular dynamics simulation of the same molecule embedded in a lipid bilayer. Although no pharmaceutical applications of $(\text{CF}_3)_2\text{-BA}$ and $(\text{CF}_3)_2\text{-PhA}$ have been reported to our knowledge, we point out that even smaller fluorinated molecules can be potent drugs. For example, halothane ($\text{CF}_3\text{-CHBrCl}$) is a widely used anesthetic, while the structurally similar hexafluoroethane ($\text{CF}_3\text{-CF}_3$) does not have similar potency, probably due to different behavior in

cell membranes.^{65,66} The reported pK_a values of $(CF_3)_2\text{-BA}$, $(CF_3)_2\text{-PhA}$, and $(CF_3)_2\text{-BBA}$ are as low as 3.3, 4.0, and 3.2, respectively. Therefore, only the deprotonated anionic forms of the six-spin compounds are expected to be present, even when embedded in a lipid bilayer. The six-spin system molecules were incorporated in bilayers composed of dimyristoylphosphatidylcholine (DMPC) and prepared as macroscopically oriented NMR samples.

It is not always trivial to predict the dipolar ^{19}F -NMR patterns of single-pulse and CPMG multipulse ^{19}F -NMR experiments. The dipolar coupling of a two-spin system produces a straightforward doublet, while the three-spin system within a single CF_3 label produces a simple triplet line shape. Upon moving to a six-spin system, however, the line shapes become much more complicated, as demonstrated for several well-characterized examples of small organic substances dissolved in nematic liquid crystals.^{34–37} Analysis of the observed complex ^{19}F -CPMG spectra can in principle yield precise values for the underlying dipolar coupling values, both within each CF_3 group and between adjacent CF_3 groups. We will refer to these as “residual” dipolar couplings in the sense of “partially averaged” dipolar couplings common in strongly aligned liquid crystals, which is a somewhat broader concept than what is used for weakly aligned samples in structural studies of soluble proteins, but describes the same averaging processes. These couplings will thus be useful to determine elements of the local orientational order matrix for the effectively rigid molecular fragments containing the CF_3 groups. However, the magnitudes and signs of components of the local order matrices depend on the dynamics and translational distribution of the probe molecules in the lipid bilayers. Making common assumptions about the ordering potential acting on the molecule, we were able to construct a model for the probability distribution of orientations of $(CF_3)_2\text{-BA}$ within the lipid bilayer. This comprehensive molecular description is then also compared with the results of a molecular dynamics simulation.

2. EXPERIMENTAL METHODS

A. Sample Preparation. The hexafluorinated substances 3,5-bis(trifluoromethyl)benzoic acid [$(CF_3)_2\text{-BA}$, Acros Organics, Geel, Belgium]; 3,5-bis(trifluoromethyl)phenylacetic acid [$(CF_3)_2\text{-PhA}$, Aldrich, St. Louis, MO]; 2-[3,5-bis(trifluoromethyl)benzoyl]benzoic acid [$(CF_3)_2\text{-BBA}$, Fluorochem, Derbyshire, UK] were purchased at purity >98% and used without further purification.

Oriented lipid bilayer samples were produced by codissolving the six-spin compounds (typically 0.5 mg) at a molar ratio of 5% with DMPC (Avanti Polar Lipids, Alabaster, AL) in CHCl_3 . The solution was then spread on 15 rectangular glass plates, allowed to dry in air and subsequently under vacuum overnight. To obtain oriented samples, the glass plates were stacked and incubated for 24 h at 48 °C under an atmosphere of 98% relative humidity obtained over a saturated solution of $K_2\text{SO}_4$. The achieved quality of orientation in the oriented bilayer samples was controlled by ^{31}P NMR and was usually very high (>90%). Figure 2 shows an example of a typical ^{31}P NMR spectrum. When following this protocol, all prepared samples showed highly reproducible ^{19}F -NMR spectra. No aging of samples was observed, even after months of storage at –20 °C.

When establishing this protocol for the acidic molecules, in some initial experiments a modification was considered to control the pH in the samples. Defined amounts of 1–10 μL of

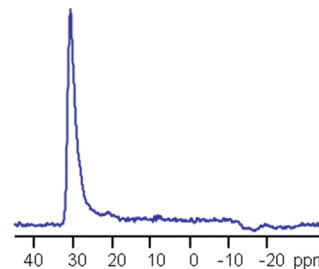


Figure 2. Oriented samples, prepared as stacks of glass plates, consistently had a high quality of alignment, as monitored by ^{31}P NMR spectroscopy. A typical phospholipid spectrum of the macroscopically aligned DMPC samples is illustrated, containing 5 mol % of the embedded six-spin substance.

concentrated buffers at different pH were added to the glass plates prior to stacking. This alternative protocol was not pursued further as it had no noticeable effect on the spectral patterns of interest, while it severely deteriorated the quality of bilayer orientation. Indeed, pH control is not expected to severely influence the samples, since the reported pK_a values suggest that only the deprotonated anionic forms will be present in the lipid bilayer.

B. NMR Spectroscopy. All NMR measurements were carried out on a 500 MHz Varian Unity Inova spectrometer equipped with a second home-built high-frequency channel for the fluorine resonance frequency of 470 MHz. For the solid-state ^{19}F -NMR measurements, a double-tuned flat-coil probe (Doty Scientific Inc., Columbia, SC) was used which allowed for proton decoupling while observing fluorine spectra. Typical lengths for fluorine 90° pulses were 2.5 μs , and proton decoupling was applied at a B_1 field strength of 15 kHz in single-pulse experiments. In CPMG experiments, dwell times of 44 μs were used, acquiring 2400 data points. For these multipulse experiments, composite 90° pulses of the type 90°_x–180°_y–90°_x were used to increase the width of spectral excitation and compensate for pulse imperfections.^{38,39} Typically, 512 scans were acquired for a single-pulse spectrum, and 4000 scans for a CPMG spectrum, with repetition delays of 3 and 5 s, respectively. A solution of NaF was used as secondary reference to calibrate spectra relative to neat CFCl_3 using reported procedures.^{11,12} No apodization was applied during processing.

C. Molecular Dynamics Simulations. The GROMOS force field was used as implemented in the GROMACS 3.0 software package⁴⁰ (see also <http://www.gromacs.org>). The simulation box contained a lipid bilayer with a total of 128 DMPC molecules (64 per layer) plus 3655 water molecules, as downloaded from http://moose.bio.ucalgary.ca/index.php?page=Structures_and_Topologies. Lipid parameters were chosen according to Berger et al.⁴¹ Water molecules were modeled as single point charge molecules.⁴² Six molecules of $(CF_3)_2\text{-BA}$ with deprotonated carboxyl groups were inserted in random orientation into the simulation box, where the necessary voids were generated by hand with the tools *editconf* and *genbox* supplied in GROMACS. A steepest-descent energy minimization of 100 steps was performed prior to simulations. Two different simulations were performed. In the first simulation (data not shown), six $(CF_3)_2\text{-BA}$ molecules were inserted in random orientations into different regions of the simulation box: two in the acyl chain region of the lipid bilayer, two in the headgroup region, and two in the interstitial water. In the second simulation, an independent simulation box was

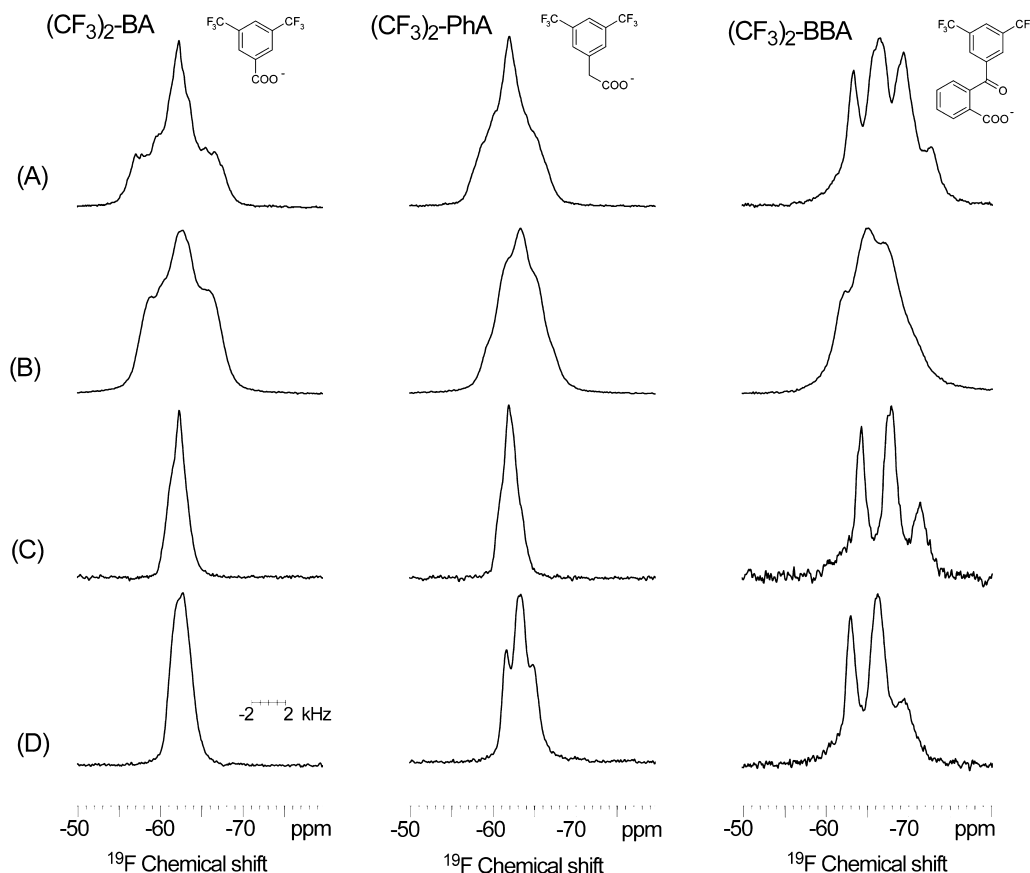


Figure 3. 470 MHz single-pulse ^{19}F -NMR spectra acquired on three different hexafluorinated model compounds dissolved in macroscopically oriented DMPC bilayers. (A) Spectra without ^1H decoupling at 35 °C, (B) same at 10 °C, (C) spectra with ^1H decoupling at 35 °C, and (D) same at 10 °C.

created, into which all six $(\text{CF}_3)_2\text{-BA}$ molecules were placed in random orientations in the lipid headgroup region. No charge compensation was introduced to neutralize the negatively charged deprotonated carboxyl groups. The second simulation covered 20 ns, using a leapfrog integration algorithm with a time step of 2 fs. Temperature and pressure were kept constant at a temperature of 343 K and a pressure of 1 bar, respectively, by weak coupling⁴² with coupling constants of $\tau_{\text{T}} = 0.1$ ps and $\tau_{\text{p}} = 1$ ps. Long-distance interactions were treated with a twin-range cutoff, using a cutoff radius of 1.8 nm for Coulomb interactions and 1 nm for van der Waals interactions. Positions were saved every 250 steps for data analysis. Angles describing the molecular orientation were calculated by basic vector calculations applied to the extracted molecular coordinates.

3. RESULTS AND DISCUSSION

A. Single-Pulse ^{19}F -NMR Experiments. The three six-spin model substances were incorporated in macroscopically oriented bilayers of dimyristoylphosphatidylcholine (DMPC), and the sample was aligned with the membrane normal parallel to the static magnetic field direction B_0 . Figure 3 shows single-pulse ^{19}F -NMR spectra obtained in the lipid gel state at 10 °C, and in the liquid crystalline phase at 35 °C. The signals are observed in the region between −60 and −70 ppm (relative to $\text{CFCl}_3 = 0$ ppm), as expected for typical isotropic ^{19}F -NMR chemical shifts of CF_3 groups.⁴³ Included in Figure 3 is a bar of 4 kHz length to illustrate the corresponding dipolar frequency scale on our 500 MHz spectrometer. Spectra acquired without ^1H decoupling are given in Figure 3, A and B. They show broad

humps of approximately 6 kHz width, with only a few spectral features resolved. At 35 °C, due to increased motional averaging of the molecules, slightly more spectral detail becomes apparent than at 10 °C, and especially the $(\text{CF}_3)_2\text{-BBA}$ spectrum now shows four resolved components. Nevertheless, we may note that the phase state of the lipids has surprisingly little effect on the dynamic behavior of these hydrophobic, membrane-embedded solutes.

Applying ^1H decoupling during acquisition narrows the resonances, but no additional spectral detail is resolved (Figure 3C,D). The spectrum of $(\text{CF}_3)_2\text{-BA}$ shows a single line of about 3 kHz width, while in $(\text{CF}_3)_2\text{-PhA}$ and $(\text{CF}_3)_2\text{-BBA}$ triplet features are discernible that are 3 and 5 kHz wide, respectively. Spectra acquired in $90^\circ-\tau-180^\circ-\tau$ spin-echo experiments (data not shown) were virtually identical to the single-pulse line shapes of Figure 3. The optimal ^1H -decoupling field was found at a very moderate strength of 15 kHz. Higher decoupling power would very likely generate temperature gradients over the sample, and the detrimental effect of sample heating nullifies the advantageous effect of increased decoupling power. Thus, the spectra of Figure 3 may possibly be improved further by reduced sample heating in a low- E probe, or in more sophisticated decoupling schemes as the CPMG multipulse sequence (see below). The observed line shapes are far narrower than those of CF_3 groups in polycrystalline environment,⁴³ and they are not perfectly symmetric triplets, as was previously observed on CF_3 -labeled peptides which showed evidence of differential relaxation.^{18,19}

The single-pulse spectra give information about the spin system present in each molecule. Rapid rotation about the $\text{C}-\text{CF}_3$

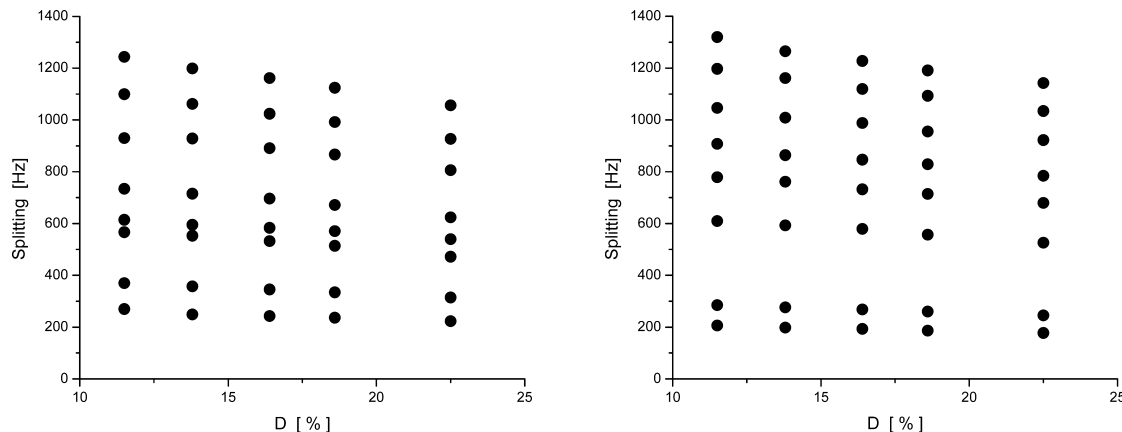


Figure 4. CPMG splittings observed on eight prominent resonances as a function of duty cycle D , in $(CF_3)_2\text{-BA}$ (left) and $(CF_3)_2\text{-PhA}$ (right).

bond makes the three fluorine nuclei in each CF_3 group magnetically equivalent in all three compounds. In $(CF_3)_2\text{-BA}$ the overall molecular structure has a C_{2v} symmetry, in which the two CF_3 groups are chemically equivalent and form an $A_3A'_3$ spin system. Rapid averaging about the C–C bond connecting the $-\text{CH}_2\text{-COO}^-$ group to the benzene ring can also make the two CF_3 groups in $(CF_3)_2\text{-PhA}$ chemically equivalent, and they are indeed seen to behave like an $A_3A'_3$ system. The situation for $(CF_3)_2\text{-BBA}$ is different. The single-pulse spectra for this molecule reveal a chemical shift difference for the two CF_3 groups, which are therefore not structurally equivalent. This spectrum corresponds to an A_3B_3 spin system, having different chemical shift values $\delta_A \neq \delta_B$ in each CF_3 group, and residual dipolar couplings $D_{AA} \neq D_{BB}$.

B. CPMG Scaling Factor in the Case of Six Strongly Coupled ^{19}F Nuclei. The single-pulse experiments have shown whether there are chemical shift differences between the two CF_3 groups, but they have insufficient resolution to yield values of the residual dipolar couplings. These were obtained from CPMG (Carr–Purcell–Meiboom–Gill) experiments which remove chemical shift differences between resonant spins, and refocus coupling to nonresonant nuclei, which in these molecules are the protons. The CPMG experiment also has the advantage of removing the effects of inhomogeneities in the static magnetic field and therefore giving narrower lines. There is one disadvantage to the CPMG experiment: although the frequencies of the lines from the resonant ^{19}F nuclei should not be changed by the CPMG sequence when ideal pulses are used, in practice it has been observed that there is a uniform scaling of the frequencies in experiments on single-spin systems. This scaling is dependent on the duty cycle, $D = t_w/\delta$, where t_w is the duration of the 180° pulses and δ is the time between these pulses in the sequence. Thus, Engelsberg and Yannoni⁴⁴ found that the dipolar splitting, Δ_{exp} , observed in a CPMG experiment applied to a pair of ^{13}C nuclei in solid samples of diluted, doubly ^{13}C -labeled acetic acid and benzene, follows the relationship

$$\Delta_{\text{exp}} = (1 - \alpha D)\Delta_0 \quad (1)$$

where Δ_0 is the unscaled dipolar splitting, and the scaling factor α was determined experimentally to be 1.0.^{25,44} The same scaling behavior has also been noticed for the single observed splitting of the ^{19}F resonances of a CF_3 group subject to a CPMG sequence by Grage and Ulrich,²⁶ who found a value of $\alpha = 1.10$. In the present cases there are two CF_3 groups and at

least two dipolar interactions present in each molecule. The scaling produced by the CPMG sequence was thus examined by recording spectra of oriented samples of $(CF_3)_2\text{-BA}$ and $(CF_3)_2\text{-PhA}$ in DMPC bilayers for a wide range of duty cycles D . Eight lines were picked that were narrow and well-resolved and could be distinctively identified in each spectrum. The splittings observed on the selected eight line pairs are shown as a function of duty cycle D in Figure 4. The scaling factor for such six-spin systems was determined by linear regression to be $\alpha = 1.10 \pm 0.05$ in a CPMG experiment using $90^\circ_x - 180^\circ_y - 90^\circ_x$ composite pulses.

C. Six-Spin Systems in CPMG Experiments. After experimental determination of the scaling factor, the six-spin systems were further investigated using the CPMG multipulse sequence^{25,26} which suppresses all nuclear magnetic interactions except for homonuclear dipolar coupling, and hence makes continuous-wave heteronuclear proton decoupling unnecessary. By correcting for the scaling factor, all spectra can be reported on an absolute frequency scale.

Experimental CPMG spectra of the three investigated six-spin systems are presented in Figure 5. At 10 and 20 °C the spectra are significantly broader than those above 30 °C, which reflects the transition to a gel phase below 23 °C. The presence of the lipid acyl chain phase transition between 20 and 30 °C was confirmed by ^{31}P NMR (data not shown), though it has remarkably little effect on the behavior of the solute molecules. The line widths are gradually seen to decrease as the temperature is raised, revealing more resolved lines: for $(CF_3)_2\text{-BA}$ and $(CF_3)_2\text{-PhA}$, the complexity of the six-spin spectral line shapes is fully discernible already at 40 °C, while $(CF_3)_2\text{-BBA}$ does not give comparable spectral resolution until 70 °C, which is partly a consequence of a more complex spin system. To ensure chemical stability of the lipids, the temperature was not raised beyond that point.

Upon tilting the oriented samples perpendicular to the magnetic field, the spectra retained their respective shapes, but were scaled down in width by a factor of 0.5 (data not shown). This behavior is consistent with the sample being in a uniaxial liquid crystalline phase, with the phase director being coincident with the sample normal. The lines show an analogous decrease in width, which indicates that the membranes are uniformly oriented. Powder components, caused by nonoriented lipid portions or solute molecules not embedded in the lipid bilayer, are present only in very minor quantities.

D. Analysis of the CPMG Spectra. Due to their complex nature, no quantitative information can be inferred by direct

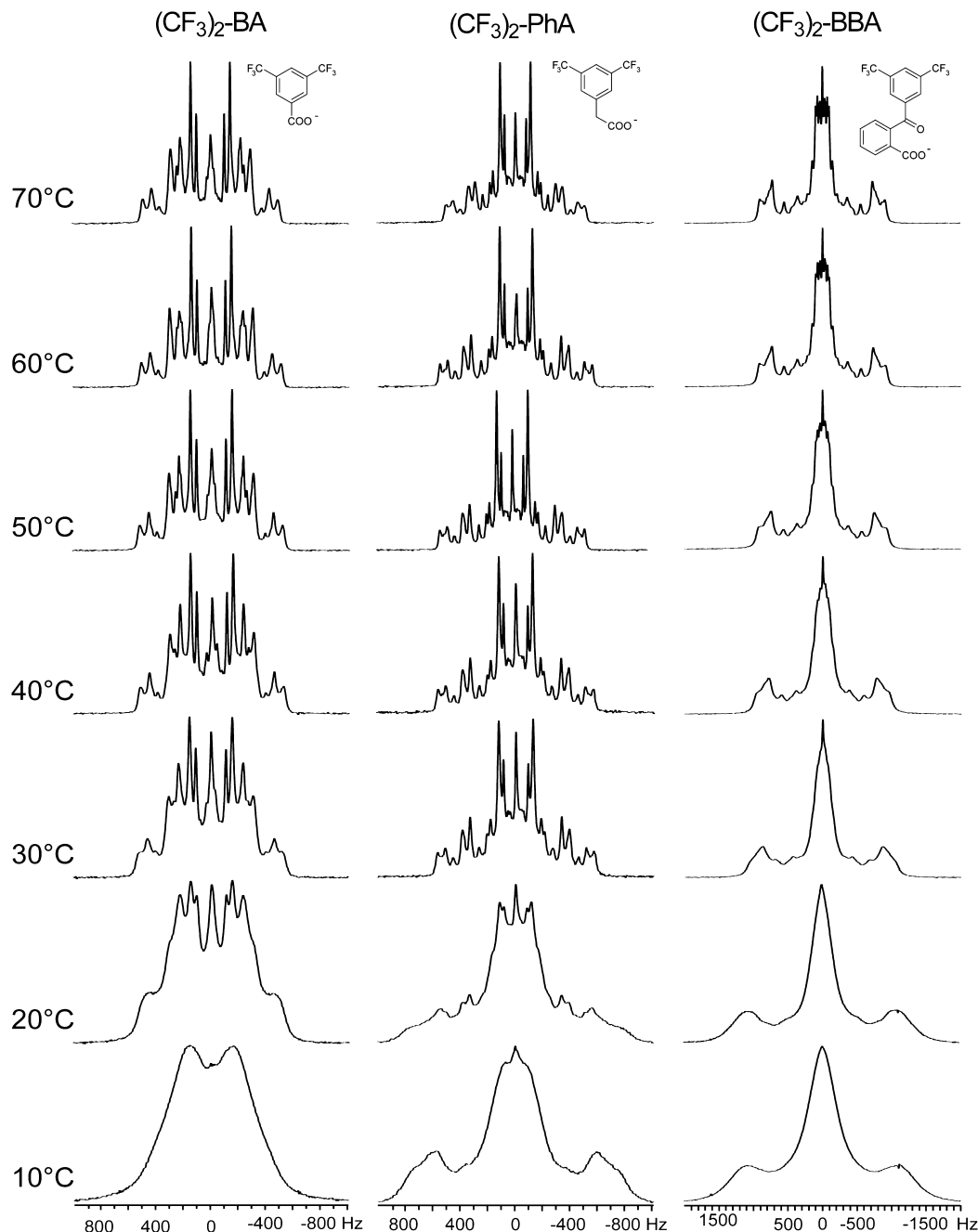


Figure 5. Pure dipolar 470 MHz ¹⁹F-CPMG spectra of 5% (mol/mol) (CF₃)₂-BA, (CF₃)₂-PhA, and (CF₃)₂-BBA embedded in macroscopically oriented bilayers of DMPC, observed over a temperature range from 10 °C (bottom) to 70 °C (top).

inspection of the CPMG spectra. In particular, no direct conclusions are possible about the underlying spin systems, unlike the situation of the single-pulse spectra in section 3A. Therefore, the peak positions observed in the CPMG spectra had to be analyzed by the iterative program ARCANA.^{45–47} For the CPMG spectra recorded at 70 °C, which had best spectral resolution, ARCANA extracted the underlying residual dipolar coupling values that are reported in Table 1. The experimental error in the values of Table 1 is dominated by the error in picking the peak positions, which is conservatively estimated to be ± 5 Hz. Therefore, the dipolar coupling values in Table 1 are quoted to ± 5 Hz accuracy. They show that the residual dipolar coupling values D_{AA} and D_{BB} are identical in (CF₃)₂-BA and (CF₃)₂-PhA, but have different values in (CF₃)₂-BBA. This confirms the

Table 1. Residual Homonuclear Dipolar Couplings between Fluorine Nuclei As Extracted by the Program Package ARCANA from CPMG Spectra Recorded at 70 °C^a

	D_{AA} (Hz)	D_{BB} (Hz)	D_{AB} (Hz)
(CF ₃) ₂ -BA	124	124	-89
(CF ₃) ₂ -PhA	150	150	-68
(CF ₃) ₂ -BBA	341	178	-58

^aThe error of each coupling value is ± 5 Hz, which corresponds to the error in locating the peak positions.

conclusion that an A₃A'₃ spin system is present in both (CF₃)₂-BA and (CF₃)₂-PhA. An A₃B₃ spin system is present, on the other hand, in (CF₃)₂-BBA, where the CPMG spectrum is not

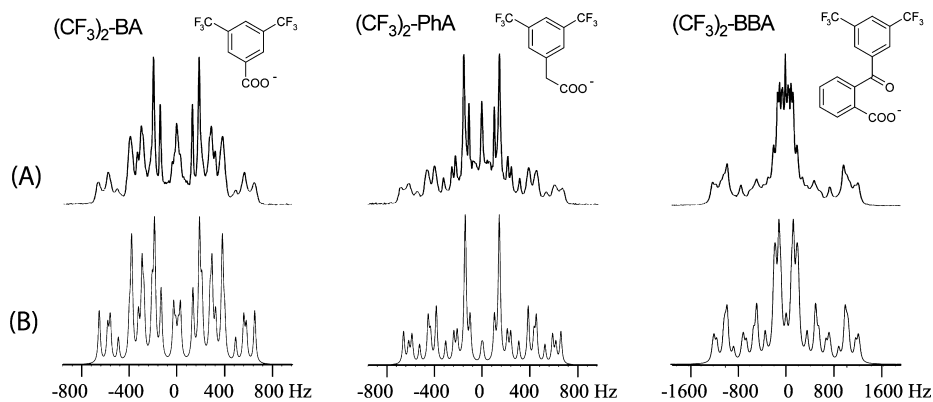


Figure 6. Comparison of experimental CPMG spectra at 70 °C (A) with the simulated spectra (B) that were calculated from the extracted dipolar coupling values.

sensitive to the chemical shift difference, but D_{AA} and D_{BB} are still different. It needs to be noted that the signed values of Table 1 are ambiguous. An inversion of all signs, resulting in negative values for D_{AA} and D_{BB} and a positive value for D_{AB} , will give rise to identical spectra. Equally, in the case of $(CF_3)_2\text{-BBA}$, an exchange of the values found for D_{AA} and D_{BB} will result in identical spectra.

E. Simulation of CPMG Spectra. As an independent verification of the dipolar analysis, the coupling values given in Table 1 were used to reproduce our spectra using the spectral simulation package SIMPSON.⁴⁸ Figure 6 compares the simulated spectra to the experimental spectra recorded at 70 °C. Resonances in the experimental spectra are narrower toward the middle of the spectra. This is attributed to the mosaic spread of the sample, which is more dominant in the outer parts of the spectrum where the orientation dependence of the splittings is strongest. This effect is not reproduced in the simulations, as they assume perfect orientation of the sample.

The simulated spectra demonstrate the high quality of the macroscopically aligned lipid bilayer samples. The observed spectra can be fully explained by a single Hamiltonian, ruling out any initial concerns that the complicated lineshapes might be caused by different molecular species (e.g., protonated and deprotonated) within the samples. In addition, the spectral components observed near zero Hz in $(CF_3)_2\text{-BA}$ and $(CF_3)_2\text{-PhA}$ are evidently part of the spectral line shape of the oriented six-spin systems, and are not due to experimental imperfections in the CPMG sequence or to incomplete macroscopic orientation of samples.

F. Relating the Residual Dipolar Couplings to Structure and Orientational Order. The residual dipolar couplings, D_{ij} , between pairs of nuclei i and j of a molecule dissolved in a liquid crystalline phase are related to structure and orientational order by

$$D_{ij} = -\frac{K_{ij}}{r_{ij}^3} [S_{zz}(3 \cos^2 \theta_{ijz} - 1) + (S_{xx} - S_{yy}) \times (\cos^2 \theta_{ijx} - \cos^2 \theta_{ijy}) + 4S_{xy} \cos \theta_{ijx} \cos \theta_{ijy} + 4S_{xz} \cos \theta_{ijx} \cos \theta_{ijz} + 4S_{yz} \cos \theta_{ijy} \cos \theta_{ijz}] \quad (2)$$

with r_{ij} the internuclear separation, measured in Å and

$$K_{ij} = \mu_0 \gamma_i \gamma_j h / 32\pi^3 \quad (3)$$

where μ_0 denotes the magnetic field constant, γ_F the gyromagnetic ratio of the fluorine nucleus, and h Planck's constant. Equation 2 with $K_{ij} = 53134.4$ Hz and r_{ij} in Å gives D_{ij} in Hz for pairs of ^{19}F nuclei. The order parameters $S_{\alpha\beta}$, $\alpha, \beta = x, y, z$, form the components of the second-rank Saupe order matrix.^{49–51} They are defined with respect to molecular axes x , y , and z fixed in a rigid part of the molecule, and are relative to the direction of the static magnetic field of the spectrometer. For the present samples this coincides with the normal of the DMPC bilayers. The angles of the type θ_{ijx} are between these reference axes and the internuclear vectors, \mathbf{r}_{ij} , which have magnitudes r_{ij} . Note that the value of K_{ij} given in eq 3 is consistent with the Hamiltonian used in ARCANA, but it is equal to half the value that is often used for defining residual dipolar couplings particularly for molecules dissolved in weakly ordering liquid crystalline solvents.

In the case of $(CF_3)_2\text{-PhA}$ and especially $(CF_3)_2\text{-BBA}$, the molecules are not rigid entities, but they show rapid exchange between multiple molecular rotamer conformations. This additional averaging process between conformers is accounted for by forming a weighted sum over the dipolar splittings corresponding to each conformation considered:

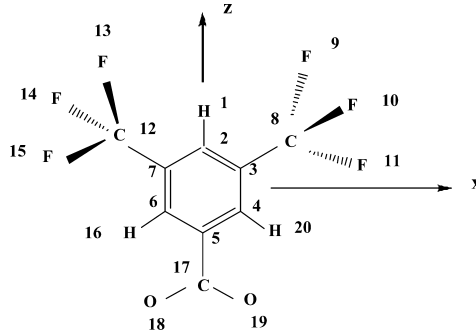
$$D_{ij} = \sum_n p_n D_{ij}^{(n)} \quad (4)$$

The additional index (n) denotes the n th molecular conformation, $D_{ij}^{(n)}$ is the dipolar splitting corresponding to the n th conformation calculated by eq 2, p_n is a weighting factor that accounts for different populations of each conformation, and D_{ij} is the experimentally observable, averaged dipolar coupling for the full system with rapid exchange between the n conformations.³⁵ In the most general case, the $D_{ij}^{(n)}$ are calculated according to eq 2, but replacing the order parameters $S_{\alpha\beta}$ by conformation specific values $S_{\alpha\beta}^{(n)}$.

So far, the couplings derived experimentally have been described as being residual dipolar couplings. However, to be exact they should be referred to as residual total anisotropic couplings, T_{ij} , which contain a contribution from the anisotropic electron-mediated spin–spin couplings, J_{ij} (aniso). The latter are negligible when the coupled nuclei involve at least one proton, but may be appreciable for pairs of ^{19}F nuclei.^{52,53} Neglecting this contribution for the current molecules may introduce an error of up to about 5%. The effect on the dipolar couplings of small-amplitude vibrational motion will also be neglected, which again may be of the order of about 5%.⁵⁴

G. Molecular Geometry and Conformational Flexibility. Detailed and well-founded assumptions of molecular geometry and conformation of the six-spin systems are needed in order to analyze experimental dipolar couplings by eqs 2–4. Namely, values for the bond lengths and angles in the solute molecules are needed, as well as the number of adopted conformations. To this end, we have calculated the geometry of $(CF_3)_2\text{-BA}$ in the minimum-energy conformation, by applying the density functional method B3LYP using a 6-311G** basis set.⁵⁵ The calculated bond lengths and angles are given in Table 2, along with a scheme that shows the used numbering of sites.

Table 2. Bond Lengths $r_{ij}/\text{\AA}$, Bond Angles θ_{ijk}/deg , and Dihedral Angles ϕ_{ijks}/deg , for $(CF_3)_2\text{-BA}$ in the Minimum-Energy Conformation, As Calculated by the B3LYP/6-311G Density Functional Method^a**



<i>i</i>	atom type	<i>j</i>	r_{ij}	<i>k</i>	θ_{ijk}	<i>s</i>	ϕ_{ijks}
1	H						
2	C	1	1.082				
3	C	2	1.395	1	120.6		
4	C	3	1.396	2	120.5	1	179.9
5	C	4	1.394	3	120.7	2	0.1
6	C	5	1.394	4	118.8	3	-0.1
7	C	6	1.396	5	120.7	4	0.0
8	C	3	1.498	2	119.3	1	2.7
9	F	8	1.362	3	112.5	2	90.0
10	F	8	1.352	3	112.8	9	120.0
11	F	8	1.360	3	112.6	9	-119.3
12	C	7	1.498	2	119.3	1	2.8
13	F	12	1.362	7	112.5	2	90.0
14	F	12	1.352	7	112.8	13	120.0
15	F	12	1.360	7	112.6	13	-119.3
16	H	6	1.084	5	117.0	4	180.4
17	C	5	1.561	4	120.6	3	179.9
18	O	17	1.248	5	114.4	4	179.2
19	O	17	1.248	5	114.4	6	179.2
20	H	4	1.084	3	122.4	2	179.7

^aThe scheme gives the numbering of sites.

It was found that rotation of the fluorine atoms in each CF_3 group about the C3–C8 or C7–C12 axes is governed in each case by a 6-fold well potential. The six equivalent rotamers have one C–F bond in each CF_3 group aligned perpendicular to the aromatic ring plane, as illustrated in Figure 7. The barrier to rotation is calculated to be 0.57 kJ/mol. For the subsequent analysis, the described local geometry and rotational potential were used for $(CF_3)_2\text{-BA}$, as well as for $(CF_3)_2\text{-PhA}$ and $(CF_3)_2\text{-BBA}$.

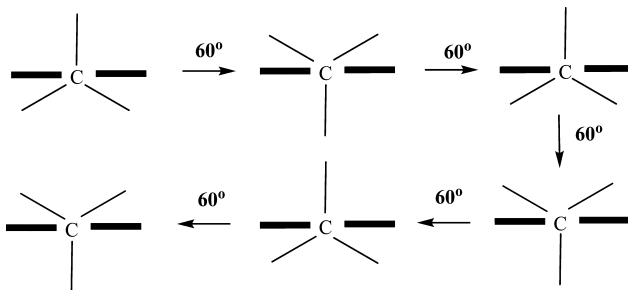


Figure 7. Isomers generated for each CF_3 group by a rotation about the $C-CF_3$ bond through successive steps of 60° .

H. Calculation of the Elements of the Saupe Order Matrix. The dipolar couplings were used to calculate the elements of the Saupe order matrix according to eqs 2 and 4 with the computer program ANCON.⁵⁶ The couplings were calculated as averages over motion between the conformations generated by rotations of the CF_3 groups: for each CF_3 group the rotation was assumed to be jumps between the six minimum-energy positions, giving a total of 36 conformations for the two CF_3 groups. The order parameters obtained are shown in Table 3. For both $(CF_3)_2\text{-BA}$ and $(CF_3)_2\text{-PhA}$, the order parameters $S_{zz}^{(n)}$ and $(S_{xx}^{(n)} - S_{yy}^{(n)})$ are independent of conformation, so that they are denoted more simply as S_{zz} and $(S_{xx} - S_{yy})$. For $(CF_3)_2\text{-BBA}$, on the other hand, the nonequivalence of the two intra- CF_3 couplings means that the value of S_{xz} must be nonzero, when averaged over all conformations of the molecule. In general, the NMR spectra yield only the relative signs of the dipolar couplings, and hence there are two possible sets of order parameters that can be obtained with their signs reversed, as shown in Table 3. The values for the components of the order matrix, especially for S_{zz} , are in a range that is typical for the headgroups and glycerol backbones of lipid bilayers.

I. Physical Interpretation of the Magnitudes of the Order Parameters. The $^{19}\text{F-NMR}$ experiments reported here yield sufficient information to obtain the order parameters given in Table 3, which describe how the molecules are aligned and distributed in the bilayer phase. The order parameters are related to the local molecular orientation according to

$$S_{zz} = Q^{-1} \int_0^{Z_b} dZ \int_0^\pi \sin \beta d\beta \int_0^{2\pi} d\gamma \left[\frac{3}{2} \cos^2 \beta - \frac{1}{2} \right] P(\beta, \gamma, Z) \quad (5)$$

$$S_{xx} - S_{yy} = Q^{-1} \int_0^{Z_b} dZ \int_0^\pi \sin \beta d\beta \times \int_0^{2\pi} d\gamma [\sin^2 \beta \cos 2\gamma] P(\beta, \gamma, Z) \quad (6)$$

with

$$Q = \int_0^{Z_b} dZ \int_0^\pi \sin \beta d\beta \int_0^{2\pi} d\gamma P(\beta, \gamma, Z) \quad (7)$$

The probability distribution, $P(\beta, \gamma, Z)$, is a function of the polar angles β and γ made by the magnetic field direction in the xyz frame, which will vary along the Z -direction of the bilayer normal; Z_b is the distance between the centers of adjacent bilayers.

The NMR experiments on the present samples cannot determine the form of the orientation–translation probability distribution function, but certain conclusions on the location of

Table 3. Components $S_{\alpha\beta}$ of the Saupe Order Matrix Extracted from the Experimental NMR Dipolar Couplings D_{ij} , and Best-Fit Values for the Interaction Coefficients $\varepsilon_{2,0}$ and $\varepsilon_{2,2}$

	D_{AA} (Hz)	D_{BB} (Hz)	D_{AB} (Hz)	S_{zz}	$(S_{xx} - S_{yy})$	S_{xz}	$\varepsilon_{2,0}/RT$	$\varepsilon_{2,2}/RT$
$(CF_3)_2\text{-BA}$	124	124	-89	0.49 ± 0.02	0.097 ± 0.004	0.0	2.326	0.668
	-124	-124	89	-0.49 ± 0.02	-0.097 ± 0.004	0.0	-34.0	-0.132
$(CF_3)_2\text{-PhA}$	150	150	-68	0.33 ± 0.01	0.033 ± 0.001	0.0	1.488 ^a	0.146 ^a
	-150	-150	68	-0.33 ± 0.01	-0.033 ± 0.001	0.0	-2.800 ^a	-0.052 ^a
$(CF_3)_2\text{-BBA}$	341	178	-58	0.187 ± 0.003	0.070 ± 0.001	0.018 ± 0.002	^b	^b
	-341	-178	58	-0.187 ± 0.003	-0.070 ± 0.001	-0.018 ± 0.002	^b	^b

^aPurely computational result, which does not take into account the conformational flexibility of the molecule. ^bFor the more complex $(CF_3)_2\text{-BBA}$ such an approach is clearly inappropriate

the solutes can be drawn from the values of the order parameters. Thus, for the present samples the spectra are consistent with the motion along Z being rapid on the time scale of the observed residual dipolar couplings. Also note that the limiting values are $-\frac{1}{2} \leq S_{\alpha\alpha} \leq 1$ for each order parameter. Solute molecules which are confined to the lipid headgroup and acyl chain regions are expected to have their major order parameter $|S_{zz}| \approx 0.2$, but if they had escaped into the aqueous layer, the absolute value of the expected order parameters would be $\ll 0.1$. The values obtained here for the three compounds therefore suggest that the molecules spend very little time, if any, in the aqueous regions between the bilayers.

J. Orientational Probability Distribution of $(CF_3)_2\text{-BA}$ in the Membrane. From the ^{19}F -NMR spectrum of $(CF_3)_2\text{-BA}$ we have derived the two order parameters S_{zz} and $(S_{xx} - S_{yy})$, based on reasonable assumptions on the molecular geometry and on the rotation of the CF_3 groups about the C-C bonds. What do these order parameters reveal now about how the molecules are situated and move in the DMPC solution? To answer this question, a model has to be chosen for the probability distribution function, $P(\beta, \gamma, Z)$. The singlet probability distribution, $P(\beta, \gamma, Z)$, is the probability that the magnetic field direction is at an orientation between $\sin \beta$ and $\sin \beta + d\beta$, and γ and $\gamma + d\gamma$, where β and γ are polar angles the field direction makes with axes fixed in a molecule, and between Z and $Z + dZ$, where Z is the position of the center of mass of a molecule along the direction of the layer normal. It is not possible to invert the experimental data in order to determine this function, but the order parameters can in principle be used to quantify aspects of proposed models. In the present case, this can be done on the basis of some simplifying assumptions, such as ignoring the Z dependence. We have strong evidence from the molecular dynamics simulation below that the $(CF_3)_2\text{-BA}$ molecules are localized entirely in the headgroup region of DMPC. The purely orientational distribution function, $P(\beta, \gamma)$, is then used to define $U(\beta, \gamma)$, the mean potential that a single molecule experiences from interactions with all other molecules in the sample (and averaged over Z):

$$P(\beta, \gamma) = Q^{-1} \exp[-U(\beta, \gamma)/RT] \quad (8)$$

where Q is a normalization factor. The potential may be expanded as

$$U(\beta, \gamma) = - \sum_{L,m} \varepsilon_{0,m}^L C_{L,m}(\beta, \gamma) \quad (9)$$

where the $C_{L,m}(\beta, \gamma)$ are modified spherical harmonics of rank $L = 2, 4, \dots, \infty$, and components $m = -L$ to L . Such an infinite sum is exact, but impractical. Retaining only the terms with $L = 2$ has been found to be a useful approximation for calculating the

averages of second-rank properties such as the Saupe order parameters.⁵⁷ The equation is further simplified when the molecule-fixed axes used are principal axes for the interaction tensor ε (and also for the order matrix). This leads to the result

$$U(\beta, \gamma) = -\varepsilon_{2,0} \frac{3 \cos^2 \beta - 1}{2} - \varepsilon_{2,2} \sqrt{\frac{3}{2}} \sin^2 \beta \cos 2\gamma \quad (10)$$

A pair of values of S_{zz} and $(S_{xx} - S_{yy})$, obtained at a temperature T, can be used to derive a pair of interaction coefficients $\varepsilon_{2,0}$ and $\varepsilon_{2,2}$, as given in Table 3. The simplest cases to interpret have $\varepsilon_{2,2} = 0$, such that $(S_{xx} - S_{yy})$ is zero. In this case, as $\varepsilon_{2,0}$ goes to positive infinity, then S_{zz} goes to unity, meaning that the molecules are all perfectly aligned with the molecular z-axis along the bilayer normal, while x and y are randomly distributed in the plane perpendicular to the normal. If $\varepsilon_{2,0}$ is negative, then increasing its magnitude leads to z being aligned in the plane perpendicular to the bilayer normal.

For the case of $(CF_3)_2\text{-BA}$, the parameters $\varepsilon_{2,0}$ and $\varepsilon_{2,2}$ were determined from the observed D_{ij} values, and they are included in Table 3. The two possible assignments for the sign of dipolar coupling leads to two sets of $\varepsilon_{2,0}$ and $\varepsilon_{2,2}$. These do not only differ in sign, but also in value. Two possible probability distributions $P(\beta, \gamma)$ for $(CF_3)_2\text{-BA}$ were calculated according to eqs 8 and 10, and are plotted in two different representations in Figure 8. The distribution derived from the first sign assignment of Table 3 shows a preferred orientation of the $(CF_3)_2\text{-BA}$ molecule along the lipid bilayer normal, with a wide spread around that preferred orientation. In contrast, the second distribution shows a preference for an alignment perpendicular to the lipid bilayer normal with a much narrower spread. Since both perpendicular alignment and narrow spread are biophysically not plausible, we conclude that the distribution shown in the top panels of Figure 8 is appropriate for our system. This distribution makes perfect biophysical sense, since it describes the solute molecule to be preferentially "upright" in the membrane, aligning its intrinsic amphiphilic profile with that of the lipid bilayer.

The C_{2v} symmetry of the $(CF_3)_2\text{-BA}$ molecule enabled the principal axes of the order matrices to be identified with the molecular xyz-axes. This is not possible, however, in the case of the molecules $(CF_3)_2\text{-PhA}$ and $(CF_3)_2\text{-BBA}$, as illustrated in Figure 9 for $(CF_3)_2\text{-PhA}$. The acetate group of the molecule is interconverting rapidly between two conformations, (a) and (b). Conformation (a) requires three order parameters to relate the dipolar couplings to structure: $S_{zz}^{(a)}$, $(S_{xx}^{(a)} - S_{yy}^{(a)})$, and

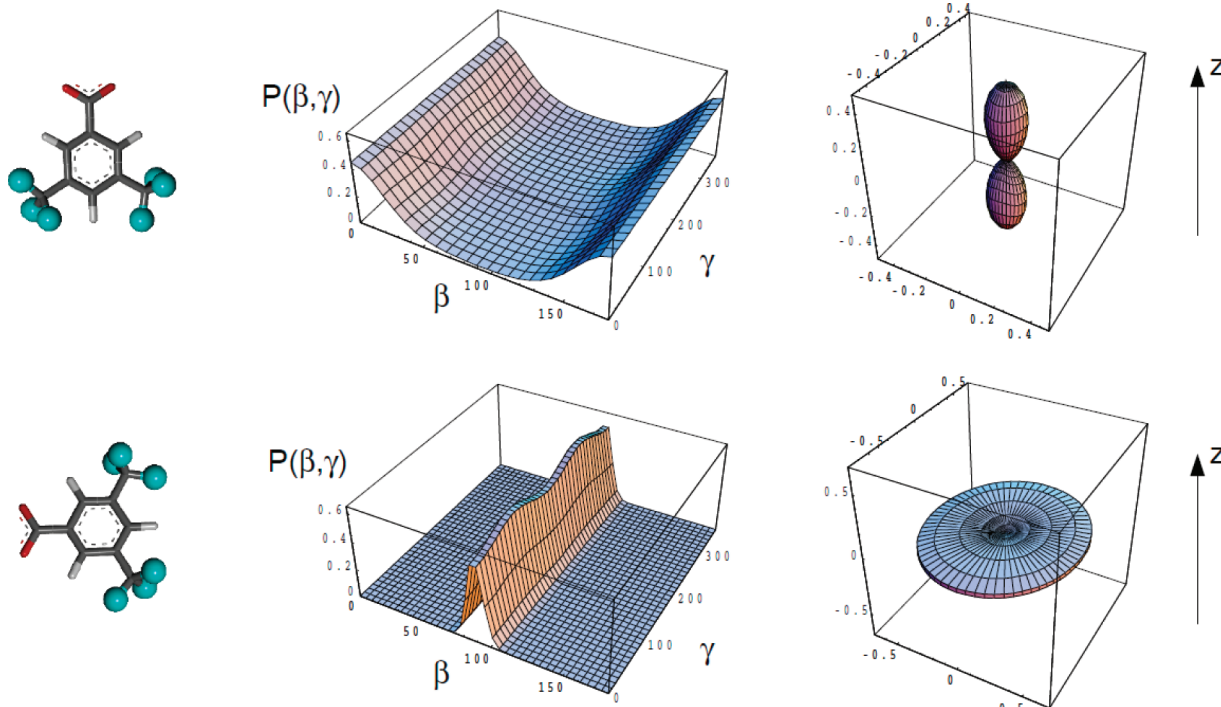


Figure 8. Probability distributions $P(\beta, \gamma)$, calculated for $(\text{CF}_3)_2\text{-BA}$ and shown in two different representations. The top and bottom rows show probability distributions calculated for the first and second alternative assignment of signs to dipolar couplings, respectively, as given in Table 3. (Left) $(\text{CF}_3)_2\text{-BA}$ shown schematically in the corresponding orientation; (center) Cartesian plots of $P(\beta, \gamma)$ over the (β, γ) -plane; (right) spherical plots with β and γ as spherical coordinates.

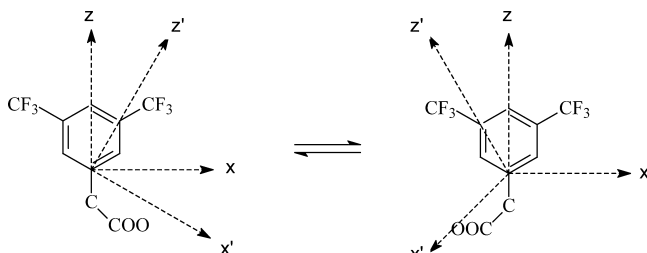


Figure 9. Two conformers of $(\text{CF}_3)_2\text{-PhA}$, illustrating the impact of interconversion between conformers. Interconversion makes the molecular frame of reference (shown unprimed) unsuitable for the analysis of NMR measurements. An intermediate frame of reference (shown primed) taking into account interconversion is necessary for analysis, but in general the relationship between molecular and intermediate frame of reference cannot be determined in a straightforward way.

$S_{xz}^{(a)}$, and there is an analogous set for conformation (b): $S_{zz}^{(b)}$, $(S_{xx}^{(b)} - S_{yy}^{(b)})$, and $S_{xz}^{(b)}$. However, symmetry demands that

$$S_{zz}^{(a)} = S_{zz}^{(b)}$$

$$(S_{xx}^{(a)} - S_{yy}^{(a)}) = (S_{xx}^{(b)} - S_{yy}^{(b)})$$

$$S_{xz}^{(a)} = -S_{xz}^{(b)}$$

Figure 9 shows intermediate frames of reference with primed axes x', y', z' that are principal axes for each of the two conformations, but their orientation relative to xyz is not known. It is not possible to use the two measured dipolar couplings to obtain the principal order parameters, and hence the principal components of the interaction tensor. Values for the interaction coefficients $\varepsilon_{2,0}$ and $\varepsilon_{2,2}$ can therefore be calculated for

$(\text{CF}_3)_2\text{-PhA}$ and are included in Table 3, but they cannot be interpreted in terms of a structural meaning.

K. Molecular Dynamics Simulation of $(\text{CF}_3)_2\text{-BA}$ in the Membrane. Two possible orientational preferences of the $(\text{CF}_3)_2\text{-BA}$ molecules within the lipid bilayer are consistent with the experimental $^{19}\text{F-NMR}$ data. In the physically more plausible situation, the $(\text{CF}_3)_2\text{-BA}$ molecules are preferentially aligned along the direction of the lipid bilayer normal, with a wide spread around that preferred orientation. It is interesting to compare this proposed orientation with the results of a molecular dynamics (MD) simulation. The GROMACS 3.0 software package⁴⁰ was used to calculate MD trajectories of six $(\text{CF}_3)_2\text{-BA}$ molecules in a box of 128 DMPC and 3655 water molecules. In a first explorative run, the six molecules were placed in random orientations into different regions of the box of lipids. Two molecules were placed in the aqueous phase, two in the lipid headgroup region, and two in the hydrophobic region of the lipid acyl chains. During a 10 ns simulation run, all molecules showed a strong tendency to move into the lipid headgroup region, and they reached a constant value of immersion depth (data not shown). This finding justified a second run with an independently generated simulation box in which all six molecules were placed in random orientation into the headgroup region from the start, with three molecules in each monolayer.

In this second run of 20 ns simulation time, all molecules retained their starting location in the lipid headgroup region. The immersion depth Z into the lipid bilayer was monitored as criterion for equilibration. After a period of 3 ns, all six solute molecules showed constant immersion depths and the expected “upright” orientation, fully supporting our choice of the appropriate probability distribution. The hydrophilic carboxyl groups project along the membrane normal toward the aqueous

phase and make full contact with the polar lipid headgroups, while the bis-CF₃ groups point toward the hydrophobic bilayer interior. Notably, the (CF₃)₂-BA molecules are located quite far up in the lipid headgroup region, with little contact between the hydrophobic CF₃ moieties and the acyl chains. This location can explain our earlier observation that the NMR spectra of the solutes (see Figures 3 and 5) are hardly affected by the main bilayer phase transition, in which the lipid acyl chains experience dramatic changes in mobility. A representative snapshot of the full simulation box at 15.85 ns simulation time is shown in Figure 10. For none of the six (CF₃)₂-BA molecules

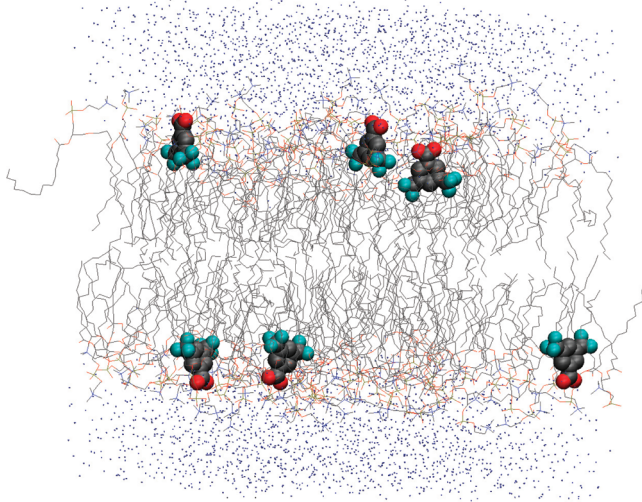


Figure 10. Snapshot of the MD simulation box at a time of 15.85 ns within the second run, showing an “upright” orientation for all six simulated (CF₃)₂-BA molecules. The lipid acyl chains are shown as gray lines in the center of the figure, the headgroup regions are shown as red and blue lines, and the water molecules are blue spheres.

any dimerization nor any other contacts were observed. Note that the two molecules on the right side of the upper layer are not in actual proximity, but are separated in the direction of the paper plane, i.e., the apparent “contact” is not real. The molecule on the right-hand side of the upper layer shows deeper immersion depth than the other molecules; this observation reflects that each molecule samples a range of immersion depths during the simulation time. The rotation of the CF₃ groups around their axis of symmetry was clearly reproduced in the simulation run, whereas the rotational diffusion of the entire (CF₃)₂-BA molecules around the membrane normal was not averaged within the 20 ns duration of our simulation.

L. Molecular Tilt and Probability Distribution of (CF₃)₂-BA in the Membrane. The (CF₃)₂-BA molecules are preferentially oriented upright in the membrane; that is, their most strongly aligned axis, z , tends to be aligned parallel rather than perpendicular to the bilayer normal, as shown in Figure 10. The values of the tilt angle, τ , between z and the bilayer normal were extracted from the second simulation run, as previously demonstrated for a related system.⁵⁸ The fully equilibrated portion of our second simulation between 3 and 20 ns simulation time was used to generate a plot of the relative frequency of tilt angle τ for each of the six molecules, as presented in Figure 11. Note that the τ values of the molecules in the upper monolayer are equivalent to $(180^\circ - \tau)$ in the lower monolayer, due to bilayer symmetry. The frequency plots show broad distributions with maximum τ values around

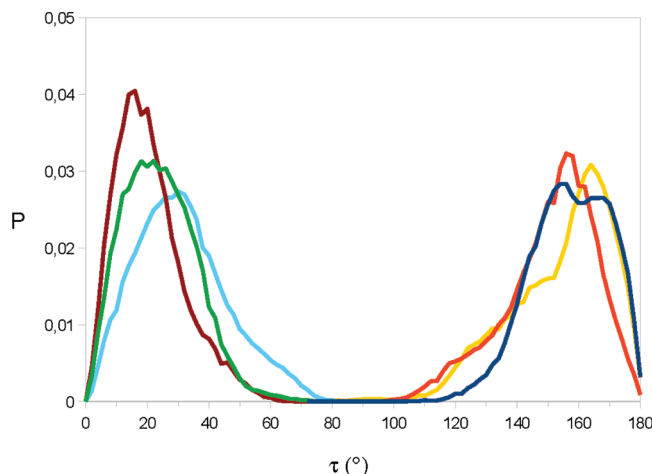


Figure 11. Relative frequency of tilt angle τ from 3 to 20 ns simulation time in the second MD run. Colors distinguish the curves for each of the six (CF₃)₂-BA molecules, where three molecules are placed in each monolayer.

15°–30° (or 150°–165°, respectively). A normalized sum of all six frequency curves was calculated and is shown as red line in Figure 12. This curve has a sharper and more symmetric shape with maxima at $\tau = 20^\circ$ and 160° .

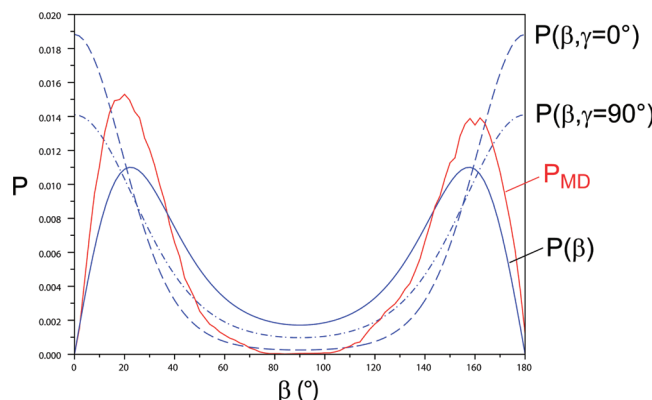


Figure 12. Normalized probability distribution curves of (CF₃)₂-BA for $\epsilon_{2,0}/RT = 2.326$ and $\epsilon_{2,2}/RT = 0.668$. The probability of the molecule to assume a specific tilt β regardless of γ [i.e., $P(\beta)$, straight line] is qualitatively different from the probability to find a specific β for a fixed value of γ [shown are $P(\beta, \gamma=0^\circ)$, dashed line, and $P(\beta, \gamma=90^\circ)$, dash-dotted line]. See text for details. Shown in red is the sum of the relative frequencies of tilt angle observed in the second molecular dynamics simulation.

The observation of a nonzero average tilt angle, $\langle \tau \rangle \neq 0^\circ$, in the trajectories may at first sight seem to contradict the conclusion made above: i.e., the orientational probability distribution $P(\beta, \gamma)$ given by eq 8 and shown in the top panels of Figure 8 was assumed to have its maximum at $\tau = 0^\circ$. The relationship between $\langle \tau \rangle$ and τ is demonstrated in Figure 12, where $P(\beta, \gamma)$ is shown as a function of β for values of $\gamma = 0^\circ$ (dashed line) and $\gamma = 90^\circ$ (dash-dotted, both lines calculated with our values of $\epsilon_{2,0}/RT = 2.326$ and $\epsilon_{2,2}/RT = 0.668$). Both curves are normalized and thus give the probability for the molecule to assume a tilt angle β for the given value of γ (which is the azimuthal angle around the rim of the cone addressed by the angle β in the probability distribution). This specific probability is different from the overall probability $P(\beta)$ to

find a molecule with a tilt angle β regardless of its actual value of γ . The probability $P(\beta)$ corresponds to the frequency plots of Figure 11 and can be inferred from $P(\beta, \gamma)$ by a definite integral over γ that accounts for spherical geometry by an angular weighting factor $\sin(\beta)$:

$$P(\beta) = \int_0^{2\pi} d\gamma \sin \beta P(\beta, \gamma) \quad (11)$$

This definite integral was convoluted with the model probability distribution $P(\beta, \gamma)$ of $(CF_3)_2\text{-BA}$. The resulting normalized $P(\beta)$ is shown as continuous blue line in Figure 12. In contrast to the specific $P(\beta, \gamma)$, the overall function $P(\beta)$ now has maxima not at zero tilt, but around $\beta = 22^\circ$ and $\beta = 158^\circ$, at slightly higher tilt angles than what was observed in the simulated frequency plot (red line in Figure 12). Also, the model distribution is broader than the simulated distribution and has higher values for β around 90° . It is a general observation in mobile systems that the time-averaged orientation $\langle \beta \rangle$ is not observed at the minimum at $\beta = 0^\circ$ of the potential function, eq 10, but due to spherical geometry occurs at a “tilted” value of $\langle \beta \rangle \neq 0^\circ$.⁵⁹

M. Comparison to NMR Spectroscopic Results on $(CF_3)_2\text{-BA}$ in the Membrane. To establish a quantitative connection between the molecular dynamics simulation results and the NMR data, the molecular order parameter S_{zz} and the biaxial order parameter ($S_{xx} - S_{yy}$) were calculated from the trajectories for the molecular x -, y -, and z -axes by time-averaging according to $S_{\alpha\alpha} := \langle (3 \cos^2 \theta_{\alpha\alpha} - 1)/2 \rangle$, where $\theta_{\alpha\alpha}$ is the angle between the respective axis and the laboratory z -axis. The averaging was carried out for the fully equilibrated portion of our second simulation run from 3 to 20 ns simulation time, and the results are listed in Table 4 for the six molecules of our

Table 4. Order Parameter Values for $(CF_3)_2\text{-BA}$ in DMPC Calculated from MD Trajectories between 3 and 20 ns Simulation Time^a

molecule	S_{zz}	$S_{xx} - S_{yy}$
1	0.708	0.026
2	0.582	0.058
3	0.642	0.150
4	0.729	-0.051
5	0.791	0.066
6	0.578	-0.168
MD av of 1–6	0.67 ± 0.08	0.069 ± 0.074
exptl NMR values	0.49 ± 0.02	0.097 ± 0.004

^aExperimental values extracted from NMR spectra are taken from Table 3 and shown for comparison.

simulation (labeled 1 to 6), together with numerical averages. The individual values extracted from the six $(CF_3)_2\text{-BA}$ trajectories show a rather broad spread, consistent with what was observed in the frequency plots, but are in good agreement with values typically found in lipid bilayers.⁶⁰ The different values show that the six molecules do not behave uniformly during the 17 ns of analyzed simulation time, and longer trajectories would be necessary for an individual molecule to sufficiently sample the conformational space. However, calculating an average over the six molecules gives an almost quantitative agreement with the experimental values of Table 3, which are included also in Table 4 for comparison. The order parameters calculated for individual molecules over an MD trajectory are expected to show a wide variability. This is simply

a consequence of the small number of solute molecules: the precision of ensemble averages increases with the number of molecules. For example, several ensemble distributions were needed to fully describe the behavior of a peptide in the membrane.⁶⁷ Choosing the positive value of S_{zz} from the two sets of NMR-derived values, it is safe to conclude that the MD simulation gives a good approximation to the behavior of this solute in the bilayer.

The experimental order parameter values are found to be slightly lower than the simulated ones, which may be caused by several effects. Possibly, the use of a high temperature of 70 °C—in both our experiment and simulation—may have led to some deviation during the MD run of the reduced temperature relative to the main lipid phase transition. Other possible explanations may be found in the system itself. The bilayer system may have modes of motion with larger amplitudes on longer time scales not covered by the MD trajectory. Discontinuous changes on longer time scales cannot be strictly excluded, such as a binding equilibrium^{61,62} of the amphiphilic molecules between the lipid bilayer and interstitial water, or transient protonation of the solute and deeper immersion into the hydrophobic core.

4. CONCLUSIONS

The complicated spectral fine structure anticipated for two adjacent CF_3 groups has been experimentally observed by solid-state ^{19}F -NMR on three different hexafluorinated druglike compounds dissolved in a lipid membrane. A CPMG heteronuclear decoupling sequence was successfully employed to reach the necessary resolution. The line shapes observed in single-pulse experiments are symmetric for $(CF_3)_2\text{-BA}$ and $(CF_3)_2\text{-PhA}$, but asymmetric for $(CF_3)_2\text{-BBA}$. This observation suggests that $(CF_3)_2\text{-BBA}$ is engaged in slow conformational changes around the bonds connecting its two phenyl rings. For all three molecules, the CPMG spectra could be analyzed to obtain the partially averaged dipolar couplings.

It was possible to characterize molecular orientational order from the observed dipolar coupling values by determining the elements of the Saupe order matrix. In the case of the two asymmetric molecules, $(CF_3)_2\text{-PhA}$ and $(CF_3)_2\text{-BBA}$, the analysis ends here. For the symmetric molecule $(CF_3)_2\text{-BA}$, on the other hand, a further calculation of the potential of mean torque is possible. We thus obtained a probability distribution of the molecule in the membrane, which is consistent with the observed Saupe matrix. However, two ambiguous and contradictory results are found for this probability distribution. One shows the expected result of an “upright” solute molecule, with its hydrophilic carboxyl group pointing toward the lipid headgroup region and the hydrophobic moiety projecting into the bilayer core. The second probability distribution depicts the biophysically unreasonable situation of the aromatic molecule being oriented perpendicularly within the lipid bilayer, which can thus be excluded.

Molecular dynamics simulations confirmed the intuitive expectation that the $(CF_3)_2\text{-BA}$ molecules are oriented in the lipid bilayer according to their amphiphilic properties, which also allows for favorable hydrogen bonding within the lipid headgroup region. The simulations show a peak in the relative frequency of molecular tilt angles at $\langle \tau \rangle = 20^\circ$, which is fully consistent with $\tau = 0^\circ$ being the minimum of the potential and the maximum of the orientational probability distribution. Values for molecular order parameters could be extracted both from the CPMG spectra and from the MD simulation, as

listed in Table 4. The experimental and simulated values are in good agreement, with simulation values slightly larger than the experimental ones. The absolute values are well in the range expected for molecules located in the lipid headgroup region, which is the most ordered region of the lipid bilayer.⁶⁰ Anisotropic molecular mobility of the flat, aromatic $(\text{CF}_3)_2\text{-BA}$ molecule is clearly present in the MD trajectories according to the data in Table 4. The biaxial order parameter ($S_{xx} - S_{yy}$) of 0.069 found in the simulation is very close to the one of 0.097 determined experimentally. Earlier studies had also reported comparable results in experimental and simulated values.^{58,63}

With regard to future applications, this study has provided some valuable insights on the potential of $^{19}\text{F-NMR}$ when applied to druglike compounds and possibly also to membrane-bound peptides. The spectral line shapes of two interacting CF_3 groups show remarkable sensitivity toward molecular geometry and dynamics. Given that appropriate software tools are available, the spectral analysis and extraction of order parameters can be performed in a straightforward manner; hence two interacting CF_3 groups can now be routinely employed as molecular reporters. A comparatively simple and biologically relevant application would be to study (homo)dimerization in membranes using CF_3 -labeled monomers. Symmetry in this case will reduce the number of geometric parameters to two (angle of the CF_3 -symmetry axis, plus the distance, as in the case of $(\text{CF}_3)_2\text{-BA}$), which makes it possible to extract more than one structural parameter using the methods presented here. This approach would thus be superior to a simple measurement of the dipolar coupling between two monofluorine substituents, yielding only one structural parameter.^{1,64} When using monofluorine substituents, a complication often lies in the need to characterize the alignment of the ^{19}F CSA tensor in the molecular frame. This problem can be avoided by suppressing the chemical shift anisotropy using the CPMG sequence. Higher-order oligomers, consisting of monofluorine labeled monomers, should thus become accessible to analysis. Highly relevant biological systems of interest have already been prepared and studied by $^{19}\text{F-NMR}$, such as the homotetrameric transmembrane portion of the M2-channel from influenza A virus.^{31,32} Employing a pair of CF_3 groups as molecular reporters may yield substantially more information.

AUTHOR INFORMATION

Corresponding Author

*E-mail: anne.ulrich@kit.edu. Tel.: +49 721 608 43222. Fax: +49 721 608 44823.

Present Addresses

¹INFAI GmbH, Gottfried-Hagen-Str. 60–62, 51105 Cologne, Germany.

[#]BOS Obernburg, Dekaneistr. 5–9, 63785 Obernburg, Germany.

Notes

The authors declare no competing financial interest.

ACKNOWLEDGMENTS

The authors express their thanks to Dr. Stephan Grage and Dr. Thierry Azais for their participation in establishing experimental conditions and sample preparation protocols. Financial aid from the Centre for Design and Structure in Biology (CDSB), Jena, is gratefully acknowledged, and from the DFG-Center for Functional Nanostructures (E1.2) in Karlsruhe.

REFERENCES

- Salgado, J.; Grage, S. L.; Kondejewski, L. H.; Hodges, R. S.; McElhaney, R. N.; Ulrich, A. S. *J. Biomol. NMR* **2001**, *21*, 191–208.
- Strandberg, E.; Ulrich, A. S. *Concepts Magn. Reson. A* **2004**, *23*, 89–120.
- Wi, S.; Sinha, N.; Hong, M. *J. Am. Chem. Soc.* **2004**, *126*, 12754–12755.
- Ulrich, A. S.; Wadhwani, P.; Dürr, U. H. N.; Afonin, S.; Glaser, R. W.; Strandberg, E.; Tremouilhac, P. P. Y.; Sachse, C.; Berditchevskaya, M.; Grage, S. L. Solid-state ^{19}F -nuclear magnetic resonance analysis of membrane-active peptides. In *NMR spectroscopy of biological solids*; Ramamoorthy, A., Ed.; CRC Press: Boca Raton, FL, 2004; pp 215–36.
- Ulrich, A. S. *Prog. Nucl. Magn. Reson. Spectrosc.* **2005**, *46*, 1–21.
- Kim, S. J.; Cegelski, L.; Preobrazhenskaya, M.; Schaefer, J. *Biochemistry* **2006**, *45*, 5235–5250.
- Patti, G. J.; Kim, S. J.; Yu, T.-Y.; Dietrich, E.; Tanaka, K. S. E.; Parr, T. R. Jr.; Far, A. R.; Schaefer, J. *J. Mol. Biol.* **2009**, *392*, 1178–1191.
- Marsh, E. N.; Buer, B. C.; Ramamoorthy, A. *Mol. Biosyst.* **2009**, *5*, 1143–1147.
- Ieronimo, M.; Afonin, S.; Koch, K.; Berditsch, M.; Wadhwani, P.; Ulrich, A. S. *J. Am. Chem. Soc.* **2010**, *132*, 8822–8824.
- Koch, K.; Afonin, S.; Ieronimo, M.; Berditsch, M.; Ulrich, A. S. *Top. Curr. Chem.* **2012**, *306*, 89–118.
- Glaser, R. W.; Ulrich, A. S. *J. Magn. Reson.* **2003**, *164*, 104–114.
- Ulrich, R.; Glaser, R. W.; Ulrich, A. S. *J. Magn. Reson.* **2003**, *164*, 115–127.
- Mikhailiuk, P. K.; Afonin, S.; Chernega, A. N.; Rusanov, E. B.; Platonov, M. O.; Dubinina, G. G.; Berditsch, M.; Ulrich, A. S.; Komarov, I. V. *Angew. Chem., Int. Ed.* **2006**, *45*, 5659–5661.
- Mykhailiuk, P. K.; Afonin, S.; Palamarchuk, G. V.; Shishkin, O. V.; Ulrich, A. S.; Komarov, I. V. *Angewandte Chem. Int. Ed.* **2008**, *47*, 5765–5767.
- Kubyshkin, V. S.; Komarov, I. V.; Afonin, S.; Mykhailiuk, P. K.; Grage, S. L.; Ulrich, A. S. In *Fluorine in Pharmaceutical and Medicinal Chemistry: From Biophysical Aspects to Clinical Applications*; Gouverneur, V., Müllen, K., Eds.; Imperial College Press: London, 2012.
- Strandberg, E.; Wadhwani, P.; Tremouilhac, P. P. Y.; Dürr, U. H. N.; Ulrich, A. S. *Biophys. J.* **2006**, *90*, 1676–1686.
- Afonin, S.; Mykhailiuk, P. K.; Komarov, I. V.; Ulrich, A. S. *J. Pept. Sci.* **2007**, *13*, 614–623.
- Glaser, R. W.; Sachse, C.; Dürr, U. H. N.; Wadhwani, P.; Ulrich, A. S. *J. Magn. Reson.* **2004**, *168*, 153–163.
- Glaser, R. W.; Sachse, C.; Dürr, U. H. N.; Wadhwani, P.; Afonin, S.; Strandberg, E.; Ulrich, A. S. *Biophys. J.* **2005**, *88*, 3392–3397.
- Afonin, S.; Dürr, U. H. N.; Wadhwani, P.; Glaser, R. W.; Ulrich, A. S. *Top. Curr. Chem.* **2008**, *273*, 139–154.
- Afonin, S.; Grage, S. L.; Ieronimo, M.; Wadhwani, P.; Ulrich, A. S. *J. Am. Chem. Soc.* **2008**, *130*, 16512–16514.
- Wadhwani, P.; Buerck, J.; Strandberg, E.; Mink, C.; Afonin, S.; Ulrich, A. S. *J. Am. Chem. Soc.* **2008**, *130*, 16515–16517.
- Maisch, D.; Wadhwani, P.; Afonin, S.; Böttcher, C.; Koksch, B.; Ulrich, A. S. *J. Am. Chem. Soc.* **2009**, *131*, 15596–15597.
- Grasnick, D.; Sternberg, U.; Strandberg, E.; Wadhwani, P.; Ulrich, A. S. *Eur. Biophys. J.* **2011**, *40*, 529–543.
- Grage, S. L.; Ulrich, A. S. *J. Magn. Reson.* **1999**, *138*, 98–106.
- Grage, S. L.; Ulrich, A. S. *J. Magn. Reson.* **2000**, *146*, 81–88.
- Grage, S. L.; Suleymanova, A. V.; Afonin, S.; Wadhwani, P.; Ulrich, A. S. *J. Magn. Reson.* **2006**, *183*, 77–86.
- Buffy, J. J.; Waring, A. J.; Hong, M. *J. Am. Chem. Soc.* **2005**, *127*, 4477–4483.
- Ulrich, A. S. High resolution solid state NMR, ^1H , ^{19}F . In *Encyclopedia of spectroscopy and spectrometry*; Lindon, J. C., Ed.; Academic Press: New York, 2000; pp 813–25.
- Gilchrist, M. L. Jr.; Monde, K.; Tomita, Y.; Iwashita, T.; Nakanishi, K.; McDermott, A. E. *J. Magn. Reson.* **2001**, *152*, 1–6.
- Luo, W.; Mani, R.; Hong, M. *J. Phys. Chem. B* **2007**, *111*, 10825–10832.

- (32) Witter, R.; Nozirov, F.; Sternberg, U.; Cross, T. A.; Ulrich, A. S.; Fu, R. *J. Am. Chem. Soc.* **2008**, *130*, 918–924.
- (33) Grage, S. L.; Gauger, D. R.; Selle, C.; Pohle, W.; Richter, W.; Ulrich, A. S. *Phys. Chem. Chem. Phys.* **2000**, *2*, 4574–4579.
- (34) Emsley, J. W. Liquid crystals: General considerations. In *Encyclopedia of NMR*; Grant, D. M., Harris, R. K., Eds.; Wiley: New York, 1996; pp 2788–2799.
- (35) Emsley, J. W. Liquid crystalline samples: Structure of nonrigid molecules. In *Encyclopedia of NMR*; Grant, D. M., Harris, R. K., Eds.; Wiley: New York, 1996; pp 2781–2787.
- (36) Diehl, P. Structure of rigid molecules dissolved in liquid crystalline solvents. In *Encyclopedia of NMR*; Grant, D. M., Harris, R. K., Eds.; Wiley: New York, 1996; pp 4591–4602.
- (37) Algieri, C.; Castiglione, F.; Celebre, G.; De Luca, G.; Longerini, M.; Emsley, J. W. *Phys. Chem. Chem. Phys.* **2000**, *2*, 3405–3413.
- (38) Levitt, M. H.; Freeman, R. *J. Magn. Reson.* **1979**, *33*, 473–476.
- (39) Freeman, R.; Kempsey, S. P.; Levitt, M. H. *J. Magn. Reson.* **1980**, *38*, 453–479.
- (40) Lindahl, E.; Hess, B.; van der Spoel, D. *J. Mol. Model.* **2001**, *7*, 306–317.
- (41) Berger, O.; Edholm, O.; Jahnig, F. *Biophys. J.* **1997**, *72*, 2002–2013.
- (42) Berendsen, H. J. C.; Postma, J. P. M.; van Gunsteren, W. F.; DiNola, A.; Haak, J. R. *J. Chem. Phys.* **1984**, *81*, 3684–3690.
- (43) Grage, S. L.; Dürr, U. H. N.; Afonin, S.; Mikhailuk, P. K.; Komarov, I. V.; Ulrich, A. S. *J. Magn. Reson.* **2008**, *191*, 16–23.
- (44) Engelsberg, M.; Yannoni, C. S. *J. Magn. Reson.* **1990**, *88*, 393–400.
- (45) Celebre, G.; De Luca, G.; Longerini, M.; Sicilia, E. *J. Chem. Inf. Comput. Sci.* **1994**, *34*, 539–545.
- (46) Longerini, M.; Celebre, G. Liquid crystalline samples: Spectral analysis. In *Encyclopedia of NMR*; Grant, D. M., Harris, R. K., Eds.; Wiley: New York, 1996; pp 2774–2781.
- (47) Castiglione, F.; Carravetta, M.; Celebre, G.; Longerini, M. *J. Magn. Reson.* **1998**, *132*, 1–12.
- (48) Bak, M.; Rasmussen, T.; Nielsen, N. C. *J. Magn. Reson.* **2000**, *147*, 296–330.
- (49) Englert, G.; Saupe, A. Z. *Naturforsch.* **1964**, *19a*, 172–177.
- (50) Saupe, A. Z. *Naturforsch.* **1964**, *19a*, 161–171.
- (51) Saupe, A. *Angew. Chem., Int. Ed.* **1968**, *7*, 97–112.
- (52) Vaara, J.; Jokisaari, J.; Wasylshen, R. E.; Bryce, D. L. *Prog. Nucl. Magn. Reson. Spectrosc.* **2002**, *41*, 233–304.
- (53) Emsley, J. W.; De Luca, G.; Lesage, A.; Longerini, M.; Mallory, F. B.; Mallory, C. W. *Phys. Chem. Chem. Phys.* **2008**, *10*, 6534–6543.
- (54) Emsley, J. W. *Liq. Cryst.* **2010**, *37*, 913–921.
- (55) Frisch, M. J.; Trucks, G. W.; Schlegel, H. B.; Scuseria, G. E.; Robb, M. A.; Cheeseman, J. R.; Scalmani, G.; Barone, V.; Mennucci, B.; Petersson, G. A.; Nakatsuji, H.; Caricato, M.; Li, X.; Hratchian, H. P.; Izmaylov, A. F.; Bloino, J.; Zheng, G.; Sonnenberg, J. L.; Hada, M.; Ehara, M.; Toyota, K.; Fukuda, R.; Hasegawa, J.; Ishida, M.; Nakajima, T.; Honda, Y.; Kitao, O.; Nakai, H.; Vreven, T.; Montgomery, Jr., J. A.; Peralta, J. E.; Ogliaro, F.; Bearpark, M.; Heyd, J. J.; Brothers, E.; Kudin, K. N.; Staroverov, V. N.; Kobayashi, R.; Normand, J.; Raghavachari, K.; Rendell, A.; Burant, J. C.; Iyengar, S. S.; Tomasi, J.; Cossi, M.; Rega, N.; Millam, N. J.; Klene, M.; Knox, J. E.; Cross, J. B.; Bakken, V.; Adamo, C.; Jaramillo, J.; Gomperts, R.; Stratmann, R. E.; Yazyev, O.; Austin, A. J.; Cammi, R.; Pomelli, C.; Ochterski, J. W.; Martin, R. L.; Morokuma, K.; Zakrzewski, V. G.; Voth, G. A.; Salvador, P.; Dannenberg, J. J.; Dapprich, S.; Daniels, A. D.; Farkas, Ö.; Foresman, J. B.; Ortiz, J. V.; Cioslowski, J.; Fox, D. J. *Gaussian 09, Revision A.02*; Gaussian, Inc.: Wallingford, CT, 2009.
- (56) Pileo, G. Ph.D. Thesis, Universita Della Calabria, 2004–2005.
- (57) Emsley, J. W.; Heeks, S. K.; Horne, T. J.; Howells, M. H.; Moon, A.; Palke, W. E.; Patel, S. U.; Shilstone, G. N.; Smith, A. *Liq. Cryst.* **1991**, *9*, 649–660.
- (58) Hoff, B.; Strandberg, E.; Ulrich, A. S.; Tielemans, D. P.; Posten, C. *Biophys. J.* **2005**, *88*, 1818–1827.
- (59) Petersen, N. O.; Chan, S. I. *Biochemistry* **1977**, *16*, 2657–2667.
- (60) Tielemans, D. P.; Marrink, S.-J.; Berendsen, H. J. C. *Biochim. Biophys. Acta* **1997**, *1331*, 235–270.
- (61) Schwarz, G.; Stankowski, S.; Rizzo, V. *Biochim. Biophys. Acta* **1986**, *861*, 141–151.
- (62) Montich, G.; Scarlata, S.; McLaughlin, S.; Lehrmann, R.; Seelig, J. *Biochim. Biophys. Acta* **1993**, *1146*, 17–24.
- (63) Ahumada, H.; Montecinos, R.; Tielemans, D. P.; Weiss-López, B. *E. J. Phys. Chem. A* **2005**, *109*, 6644–6651.
- (64) Afonin, S.; Glaser, R. W.; Berditchevskaia, M.; Wadhwan, P.; Gührs, K.-H.; Möllmann, U.; Perner, A.; Ulrich, A. S. *Chembiochem.* **2003**, *4*, 1151–1163.
- (65) Koubi, L.; Tarek, M.; Bandyopadhyay, S.; Klein, M. L.; Scharf, D. *Biophys. J.* **2001**, *81*, 3339–3345.
- (66) Koubi, L.; Tarek, M.; Bandyopadhyay, S.; Klein, M. L.; Scharf, D. *Anesthesiology* **2002**, *97*, 848–855.
- (67) Esteban-Martin, S.; Salgado, J. *Biophys. J.* **2007**, *93*, 4278–4288.